Synergetic effects of nano-SiO$_2$/glycerol on the electrical and optical properties of PVA for embedded electronics and optical applications

Emad Mousa[1,*] ![ORCID] and Eman O. Taha[2]

[1] *Physics Department, Faculty of Science, Cairo University, Cairo, Egypt*
[2] *Petroleum Applications Department, Egyptian Petroleum Research Institute (EPRI), Cairo, Egypt*

ABSTRACT

The present study aims to prepare a low-cost, eco-friendly, free-standing film with optimized physical properties. A PVA composite of hard-soft hybrid filler ratio 1:3 (nSiO$_2$:Gl) is prepared by casting. Dynamic mechanical analyses are processed in the frequency range (0.01–9 Hz). Moreover, dielectric studies are performed in the frequency range (50 Hz–5 MHz). Herein, the modified Jonscher equation and electric modulus formalism are used to explain the results. Transmittance and reflectance of studied samples are measured in the UV–Vis range (200–700 nm). Detailed discussions of band structure, refractive index, and optoelectronic parameters are addressed. Remarkably, the results showed that mechanical and electrical properties of PVA can be tuned by careful modulation of glycerol content, whereas optical properties are more sensitive to nSiO$_2$ content. Finally, FTIR and SEM structural analyses investigate the induced structural changes in PVA.

1 Introduction

The applications of silica-based composites are extremely varied including; electronics, optical devices, optical packaging materials, photoluminescent conducting films, photoresist materials, flame-retardant materials, proton exchange membranes, anti-corrosion materials, oil adsorbents, and biomedical materials [1, 2].

It was reported in the literature that silica nanoparticles (nSiO$_2$) have a high impact on the optical properties of polymers. A considerable decrease in the band gap of polymer composite upon adding nSiO$_2$ particles is reported for pure polymer matrix [3], polymer blends [4], and hybrid polymers [5]. Moreover, nSiO$_2$ addition causes an increase in the refractive index of the composites [3, 5, 6]. Also, the light reflection at the boundaries between polymer and filler increases as the nanoparticle content in the polymer composite increases and, consequently, the transmittance of composite decreases. Deep insight tells us that optical properties of polymer

Address correspondence to E-mail: emad@sci.cu.edu.eg

composites are not affected only by particle content, but also affected by particles' type, size, and dispersion quality [7].

Therefore, polyvinyl alcohol (PVA) is a good choice as a host polymer for $nSiO_2$ particles due to its hydrophilicity that allows higher dispersion of SiO_2 in the polymeric matrix and results in a highly homogenous and optically transparent films [8]. Moreover, PVA is characterized by its biodegradability, biocompatibility, transparency, excellent emulsifying and adhesive properties, and stability against organic solvents [9, 10].

Karthikeyan et al. studies of $PVA/nSiO_2$ composite showed that PVA preserved the characteristic photoluminescence of $nSiO_2$, which suggests that this composite could be applicable for optoelectronic devices [11]. Biocompatibility and non-toxicity of amorphous SiO_2 nanoparticles ensures that $PVA/nSiO_2$ composite is environmentally friendly [12, 13].

But on the other hand, it was also reported that the dielectric properties of the $PVA/nSiO_2$ composite showed anomalous behavior [14]. The dielectric constant of the matrix decreases upon addition of $nSiO_2$ at low concentrations and then increases gradually, which is not a common behavior of polymer composites.

Improving the dielectric properties of polymer composites by adding high dielectric constant fillers is not completely satisfactory. The process requires high concentrations of filler, which consequently deteriorate the mechanical properties of the polymer itself. Instead, the addition of a third conductive phase at the percolation level enhances the dielectric constant of the composite at lower concentrations of the dielectric filler. The controlled addition of fillers avoids high dielectric losses or deterioration of mechanical properties [15].

Percolative conductive fillers used in three-phase composites include metals such as Nickel [16] and Silver [17], carbons such as nanotubes [18], fibers [19], and graphene [20], conductive polymers such as polyaniline [21], and some other inorganic materials such as radial Zinc oxide [22], and Silicon carbide [23].

Although glycerol (Gl) has been commonly used as a polymer plasticizer [24–26], some researchers have studied the effect of glycerol addition on the electrical properties of polymers. Based on impedance analysis, Ayala et al. reported that the DC conductivity of cassava starch biopolymer was very sensitive to glycerol addition up to 50 wt% [27]. On the other hand, Skov et al. studied the effect of glycerol addition on the electric and mechanical properties of hydrophobic polydimethylsiloxane (PDMS) elastomer in an attempt to obtain a novel dielectric elastomer with high dielectric constant and tunable elastic modulus [28]. Dielectric results were explained on the basis of the Jayasundere and Smith model [29].

Zakaria et al. used glycerol (Gl) as a conductive liquid filler in a three-phase composite with PDMS as the host polymer and Titanium dioxide (TiO_2) as the dielectric filler [30]. Optimum electrical and mechanical properties were attained for the hybrid filler ratio of 1:1 (TiO_2:Gl).

To the best of our knowledge, researchers who have studied glycerol's enhancement of the electrical conductivity and flexibility of different polymer composites have never studied its effect on the optical properties of these composites. Given the aforementioned distinctive optical properties of the eco-friendly $PVA/nSiO_2$ composite, it might be beneficial to enhance and tune its conductivity and flexibility through controlled addition of glycerol. Herein, the consequence of hybrid filler ($nSiO_2$:Gl) addition on the mechanical, electrical, and optical properties of PVA is a crucial point of study. The effect of individual fillers will also be studied for guidance. Afterward, the measured properties will be correlated to the induced structural changes.

In a nutshell, we aim to prepare a low-cost, eco-friendly, free-standing film with optimized physical properties to be utilized in the field of embedded electronics and optical applications.

2 Experimental

2.1 Samples preparation

PVA (Fluka, Mw = 72,000 g mol^{-1}, degree of hydrolysis 97.5–99.5 mol%) was dissolved in double distilled water by stirring at 90 °C for 1 h. To prepare plasticized composites, glycerol (Alfa Aesar, 99%) was added drop wisely to previously dissolved PVA with continuous stirring. Meanwhile, SiO_2 doped nanocomposites were prepared by ultrasonication of SiO_2 nanopowder (Sigma Aldrich, 99.5% trace metal basis, 5–20 nm particles size) in distilled water for 15 min. before being added to PVA solution and

stirred for an additional 1 h. All samples were simply cast after complete dissolution onto polystyrene Petri dishes and left to dry for 48 h at 40 °C. The content of the prepared samples is collected in Table 1.

2.2 Measurements

Dynamic mechanical properties of the samples were examined by DMA analyzer (MetraviB + 25 Instrument, France) in strain mode at ambient temperature. Samples were exposed to different oscillations of 0.01, 0.05, 0.09, 0.1, 0.5, 0.9, 1, 5, and 9 Hz.

For electrical measurements, samples were cut in the form of discs (0.2 mm in thickness and 10 mm in diameter). In addition, samples were coated with silver paste to ensure good electrical contact. The AC electrical properties were analyzed using a computer-controlled LCR bridge (HIOKI, 3532–50 LCR HiTES-TER, JAPAN) in the frequency range 50 Hz–5 MHz.

Optical investigations were performed using a (JASCO High Performance UV/VIS/NIR, model V-770) spectrophotometer in the range 200–700 nm.

Attenuated total reflection-Fourier transform infrared spectra of samples were measured in the wave number region 4000 to 600 cm^{-1} using ATR-FTIR Bruker Alpha spectrometer (Bruker Corporation, Germany) with Platinum ATR module.

Samples were analyzed by scanning electron microscope (SEM; Quanta 250 Field Emission Gun, FEI Company, Netherlands) attached with Energy Dispersive X-ray (EDAX) unit.
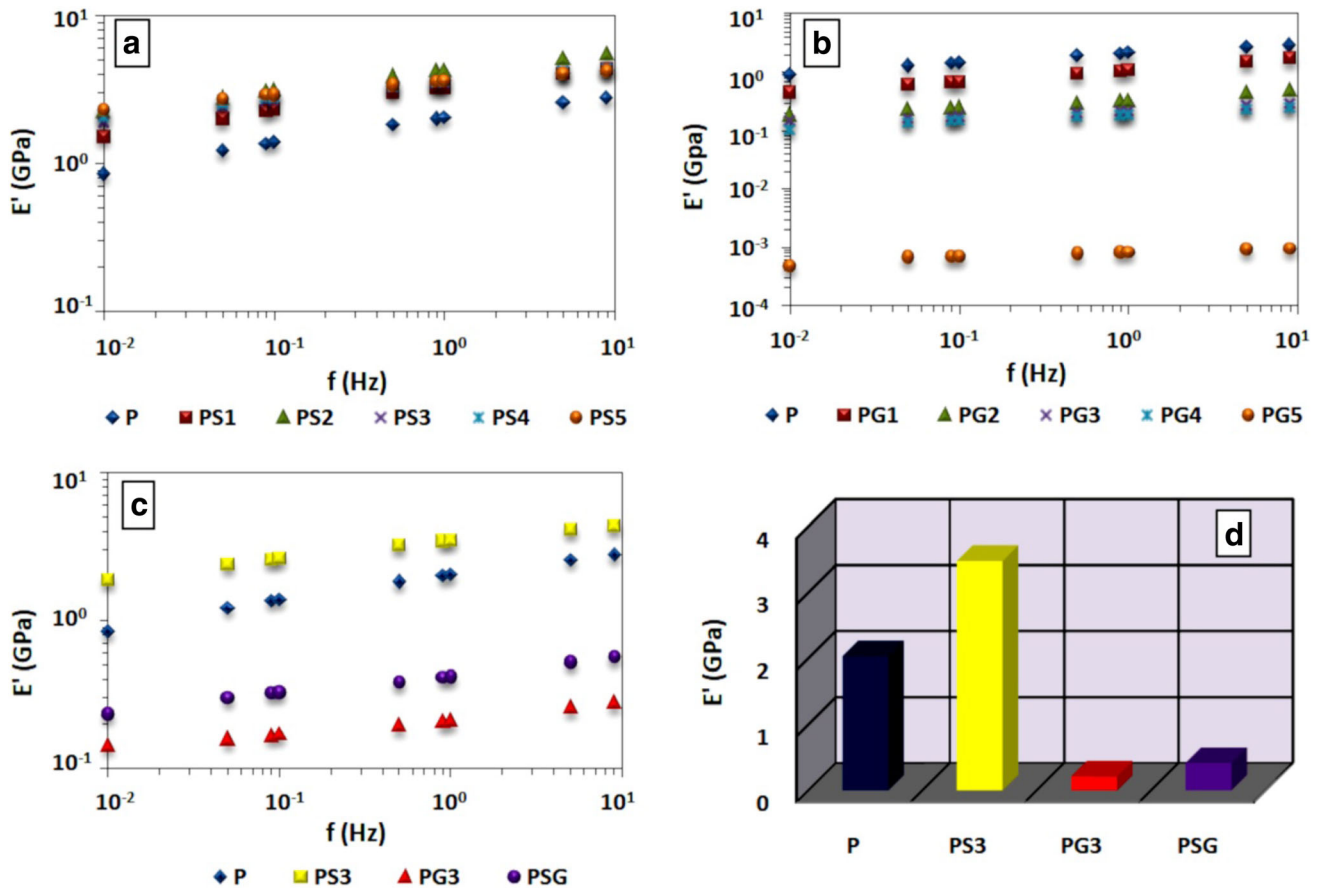
3 Results and discussion

3.1 Mechanical properties

The investigation of mechanical properties of polymer composites as a function of filler content is of great importance in polymer processing, especially for the design of processing operations and exploring structure–property relationships of polymer composites [31].

Figure 1a represents the frequency dependence of storage modulus ($E^{'}$) for PVA/nSiO$_2$ composites. A slight increase in $E^{'}$ with the increase in SiO$_2$ content (up to 5 wt%) is observed and attributed to the reduced mobility of polymer segments resulting from the strong interaction between the hydroxyl groups on silica surface with the reactive group of PVA [32]. On contrary, $E^{'}$ decreases for all PVA/Gl composites with the increase in glycerol content as depicted in Fig. 1b. Although glycerol interacts through hydrogen bonding with PVA, its plasticizing effect may be attributed to the increased spacing between PVA chains. The glycerol molecules embedded between polymeric chains create higher free volume and, consequently, higher chain mobility [25]. Furthermore, Fig. 1c demonstrates that three-phase component sample (PSG) showed a higher tensile modulus than that of purely glycerol-plasticized sample (PG3), but still plasticized with $E^{'}$ values less than those of P and PS3 samples. A comparison of $E^{'}$ values at 1 Hz for P, PS3, PG3, and PSG samples is illustrated in Fig. 1d. The high reduction in $E^{'}$ value of PSG infers that the storage modulus of the PSG sample is highly

Table 1 Content proportions of prepared samples

Sample	PVA content (wt%)	Glycerol content (wt%)	SiO$_2$ content (wt%)
P	100	0	0
PS1	99	0	1
PS2	97	0	3
PS3	95	0	5
PS4	90	0	10
PS5	85	0	15
PG1	95	5	0
PG2	90	10	0
PG3	85	15	0
PG4	80	20	0
PG5	70	30	0
PSG	85	15	5

Fig. 1 Frequency dependence of Storage modulus for **a** PVA/nSiO$_2$ composites, **b** PVA/Gl composites, **c** P, PS3, PG3, and PSG samples, and **d** P, PS3, PG3, and PSG samples at 1 Hz

affected by glycerol content rather than nSiO$_2$ content.

On the other hand, an obvious increase in $E^{'}$ with the increase in frequency was observed for all samples. Time-dependent stress will force the sample to modulate its internal molecular arrangements in order to reduce the induced localized stresses. A low elastic modulus value is the result as long as there is enough time (low frequency) for the material to complete its internal rearrangements. Meanwhile, high-frequency measurements result in high elastic modulus values [33].

### 3.2 Electrical properties

Preparing flexible polymer composites with tunable dielectric properties is crucial for embedded electronics technology [15].

Figure 2a shows the frequency dependence of real (ε') and imaginary (ε'') parts of dielectric constant of PVA/nSiO$_2$ composites. As observed in many dielectrics, all samples showed normal frequency dependence of ε'. A high polarization, and consequently ε' value, is expected at low frequency as different types of permanent and induced dipoles have sufficient time to respond to the applied electric field. As the alteration of the field increases, dipoles lag behind the field, and a consequent decrease in ε' is observed.

On contrary, ε' dependence on the nSiO$_2$ content, depicted at 1 kHz in the inset of Fig. 2a, was anomalous [4, 14].

Adding filler of high ε' to a polymeric matrix is not the only factor that controls ε' value of the resulting composite. Excluding external factors (e.g., temperature, humidity, etc.), some other factors affect ε' of polymer composites such as the shape of filler particles, filler concentration, filler size, and the nature of polymer-filler interaction [15]. It is worth noting that freely rotating dipoles have a greater participation rate in increasing the dielectric constant value than constrained ones. Therefore, in some cases, the
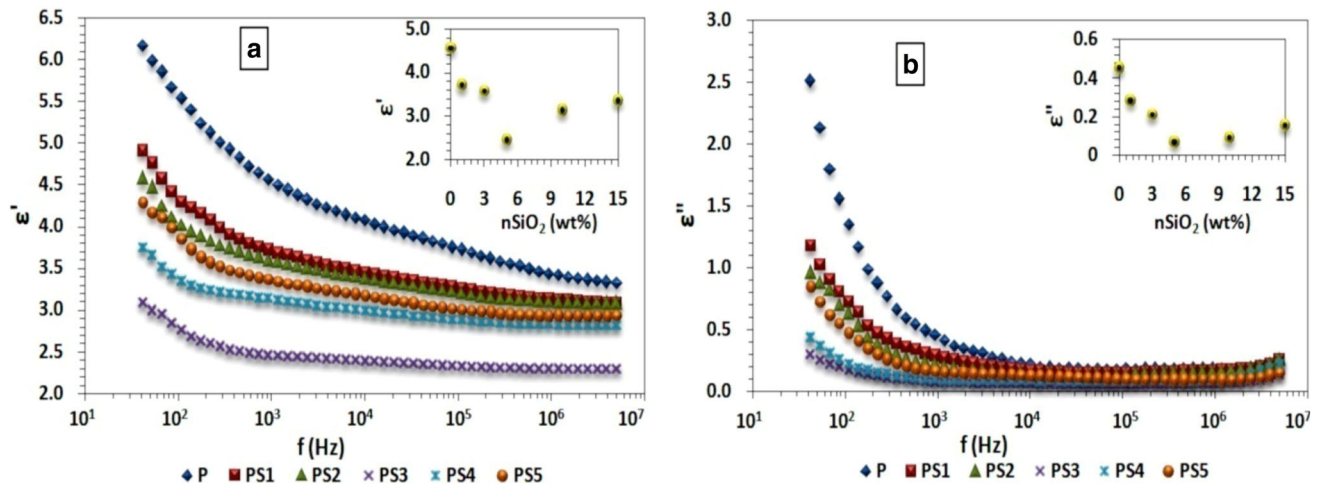
Fig. 2 a Frequency dependence of ε' for PVA/nSiO$_2$ composites, inset depicts ε' as a function of nSiO$_2$ content, and **b** Frequency dependence of ε'' for PVA/nSiO$_2$ composites, inset depicts ε'' as a function of nSiO$_2$ content

molecular conformations of the mixed constituents may disrupt the net dipolar arrangement leading to a lower value of ε' [34]. This fact may explain the reduction in ε' value with nSiO$_2$ content (up to 5% of PVA) as both the SiO$_2$ nanoparticles and PVA chains got constrained by their strong H-bonding interactions. At higher nSiO$_2$ content, silica particles tend to agglomerate and hence become less constrained by interaction with PVA chains, leading to a slight increase of ε'.

The frequency dependence of ε'' for PVA/nSiO$_2$ composites is shown in Fig. 2b. All samples do not show any relaxation peak over the scanned frequency range (50 Hz–5 MHz), and the relatively high losses at low frequency are attributed to interfacial polarization. The dependence of ε'' on nSiO$_2$ content is similar to that of ε'.

Substantially, glycerol is the constituent of the highest conductivity in our three-phase polymer composite [35]. Thus, it is essential to study the effect of glycerol addition on the conductivity of polymer matrix before proceeding to the next step. Figure 3 shows the frequency dispersion of AC conductivity (σ_{AC}) for PVA/Gl composites. The frequency spectra of σ_{AC} exhibit a DC plateau σ_{DC} at low frequency that arises mainly from uninhibited random hopping of ions [36]. Obviously, as the glycerol content exceeds the percolation concentration (≥ 15 wt% of PVA), charge carriers travel long distances through a continuous network structure of glycerol, and the DC region expands [37, 38].

The dispersion regime of σ_{AC} for sample P is successfully fitted to the well-known Jonscher equation:

$$\sigma_{AC} = \sigma_{DC} + A\omega^S \qquad (1)$$

where (A) is a temperature-dependent parameter and (S) is a power factor less than unity.

However, glycerol-loaded samples showed a super-linear behavior ($S > 1$) that did not match Eq. (1). A modified form of Jonscher power law that accounts for sub-linear ($S_1 < 1$) and super-linear ($1 \leq S_2 < 2$) behaviors is used instead.

$$\sigma_{AC} = \sigma_{DC} + A_1\omega^{S_1} + A_2\omega^{S_2} \qquad (2)$$

where (A_1) and (A_2) are temperature-dependent parameters, and (S_1) and (S_2) are power exponents related to the conduction mechanism.

Hence, the dispersion regime is described by Eq. (2) through the second term, which owes to translational hopping, and the third term, which accounts for localized hopping between neighboring sites [39].

The dependence of σ_{DC} on glycerol content is depicted in the inset of Fig. 3, while the power factors of Eqs. (1) and (2) are collected in Table 2 along with the regression values (R^2). It is clear that σ_{DC} for all PVA/Gl composites is higher than that of pure PVA. Besides, a steep rise in σ_{DC} of the composite is observed at glycerol content (≥ 15 wt%). The initial gradual increase in σ_{DC} results from increased amorphousity of PVA by glycerol addition [25]. Further, the steep rise in σ_{DC} at glycerol content (≥ 15 wt%) may be interpreted based on percolation theory; as long as glycerol content reaches a percolative

Fig. 3 AC conductivity for PVA/Gl composites. Solid lines represent fitting to Eqs. (1) and (2). Inset depicts σ_{DC} as a function of Gl content
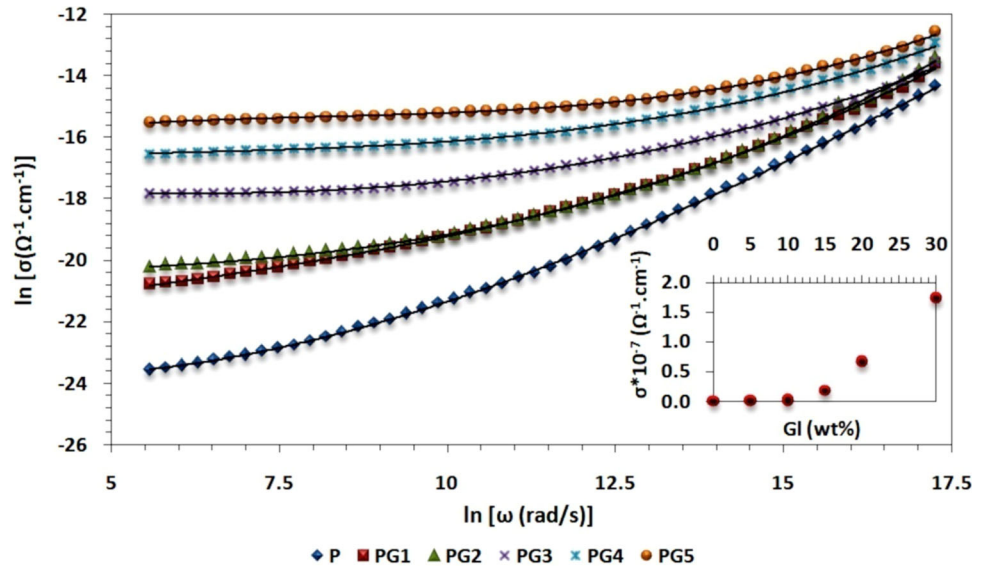
Table 2 Electrical parameters of PVA/Gl composites

Sample	S_1	S_2	R^2	M''_{max}	$f_{max}(10^4 \text{ Hz})$	$\tau(10^{-5} \text{ s})$
P	0.95	–	0.997	–	–	–
PG1	0.49	1.16	0.999	0.06	0.12	84.5
PG2	0.51	1.21	0.999	0.06	0.12	84.5
PG3	0.65	1.00	0.997	0.08	3.34	2.99
PG4	0.54	1.90	0.998	0.07	22.5	0.44
PG5	0.34	1.00	0.998	0.05	22.5	0.44

value, it forms a network structure and the conductivity of the composite increases sharply [28, 40].

In materials containing conductive components such as our investigated PVA/Gl composites, molecular relaxations may be camouflaged by conductivity effects. In this case, employing electric modulus formalism is essential to compromise the obscured relaxations [41]. The electric modulus is a complex quantity that is inversely proportional to the permittivity of the material ($M^* = 1/\varepsilon^*$) and is expressed as follows:

$$M' = \frac{\varepsilon'}{\left(\varepsilon'\right)^2 + \left(\varepsilon''\right)^2} \tag{3}$$

$$M'' = \frac{\varepsilon''}{\left(\varepsilon'\right)^2 + \left(\varepsilon''\right)^2} \tag{4}$$

where M' and M'' are the real and imaginary parts of electric modulus, respectively.

The frequency characteristics of M' for PVA/Gl composites are plotted in Fig. 4a. Clearly, small values of M' are observed for P sample at low frequencies as an indication of the negligible contribution of electrode polarization which, on the contrary, diminished completely for glycerol-loaded samples. The glycerol-loaded samples showed S-shaped behavior, which is typical for ionic materials [6]. On the other hand, Fig. 4b demonstrates M'' spectra for PVA/Gl composites. Although pure PVA does not show any relaxation peak in the measured frequency range, glycerol-loaded samples showed intense relaxation peaks, which shift to higher frequencies as the glycerol content increases. Indeed, M'' peak accounts for mobility transition from long-range hopping of carriers (at low-frequency side) to short-range hopping (at high-frequency side). The relaxation peaks for 5% and 10% glycerol-loaded samples aroused at ($\sim$ 1 kHz), suggesting that conductivity relaxations are predominated for these samples. Meanwhile, the 15% glycerol-loaded sample showed its peak around ($\sim$ 10 kHz) and the peaks of 20% and 30% glycerol-loaded samples are shifted to ($\sim$ 100 kHz). This finding suggests the existence of localized high-frequency dipolar relaxation in these samples [42].

In addition, the relaxation time (τ) corresponding to loss peak frequency (f_{max}) is deduced ($\tau = 1/f_{max}$) and gathered in Table 2. An obvious decrease in relaxation time with the increase in glycerol content reveals the acceleration of segmental chain dynamics
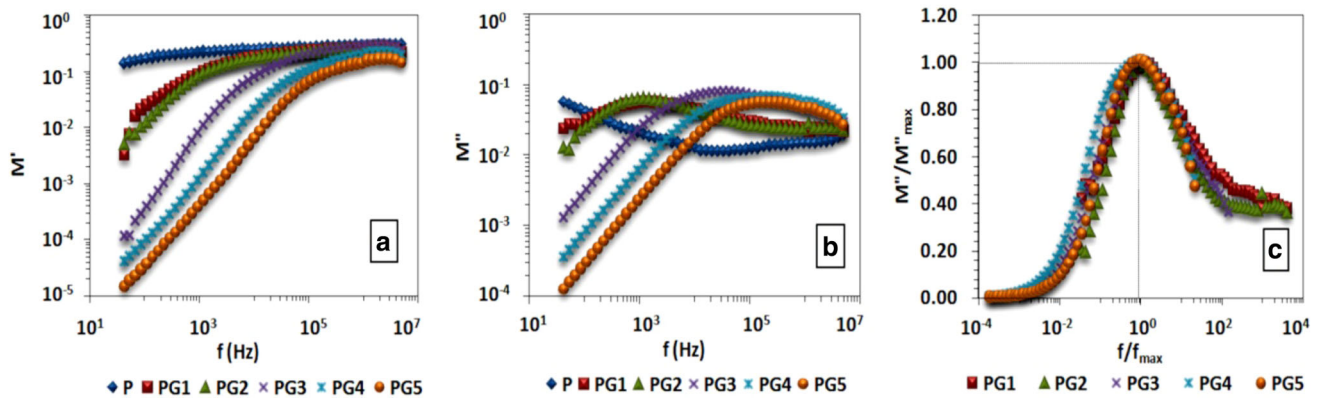
Fig. 4 **a** M' against f, **b** M'' against f, and **c** M''/M''_{max} against f/f_{max} for PVA/Gl composites

responsible for charge transportation upon glycerol addition [42].

A normalized plot of M''/M''_{max} against f/f_{max} is derived as shown in Fig. 4c to obtain a master curve of M''. The figure revealed that relaxation peaks are not identical and exhibit asymmetric broadening, which indicates non-Debye relaxation [43].

To infer how far glycerol addition affects the electrical properties of PVA/nSiO$_2$ composites, the electrical properties of P, PS3, PG3, and PSG samples are presented in Fig. 5a–e. It is obvious from figures that the electrical behavior of sample PS3 is very close to sample P, which means that nSiO$_2$ has weak effects on the electrical properties of PVA. Meanwhile, sample PSG behaved similarly to sample PG3, ensuring that glycerol's role in the electrical properties of PVA was dominant.

Samples P and PS3 attain small values of ε' and ε'', as shown in Fig. 5a and b, which decreases slightly upon increasing the frequency (up to 100 Hz). The impurities resulting from unpolymerized residues and water molecules have different conductivities than PVA chains, and thus build up of charge accumulation at the interfaces lead to the presence of Maxwell–Wagner-Sillars (MWS) interfacial polarization in sample P [44]. However, strong interaction between impurities as well as nSiO$_2$ particles and PVA matrix results in weak interfacial polarization in P and PS3 samples. As the frequency increases, the relaxation of entrapped charges at interfaces becomes slower than the change in electric field direction. Hence, such interfacial polarization ceases and results in a decrease in ε' and ε'' values. Eventually, slight frequency dispersion of polarization exhibited at low frequency owes to the weak interfacial polarization.

Meanwhile, the frequency dispersion of ε' and ε'' for PG3 and PSG samples was larger than pure PVA and continued up to 10 kHz due to interfacial and dipolar polarization. This finding suggests that glycerol molecules were highly free and facilitated the segmental motion of polymeric chains in addition to their large interfacial area.

The frequency dependence of σ_{AC}, shown in Fig. 5c, illustrates the high conductivity of PG3 and PSG samples compared to P and PS3 samples. Equation (1) was fitted to σ_{AC} plots of samples P and PS3, while Eq. (2) was utilized to extract the fitting parameters of PG3 and PSG samples. Yet, the PSG sample is slightly less conductive than the PG3 sample. Moreover, electric modulus spectra are depicted in Fig. 5d and e.

Similarly, the behavior of P and PS3 samples was almost invariant concerning each other, as also PG3 and PSG samples. The relaxation time of PSG sample extracted from Fig. 5e was a bit higher than that of PG3 sample, which owes to the limited hindrance caused by nSiO$_2$ content. Electrical parameters of P, PS3, PG3, and PSG samples are summarized in Table 3.

3.3 Optical properties

Transmission and reflection spectra represent the preliminary investigations of the optical properties of materials. Consequently, the transmittance (T%) and reflectance (R%) measurements of our samples were performed in the UV–Vis spectral range (200–700 nm).
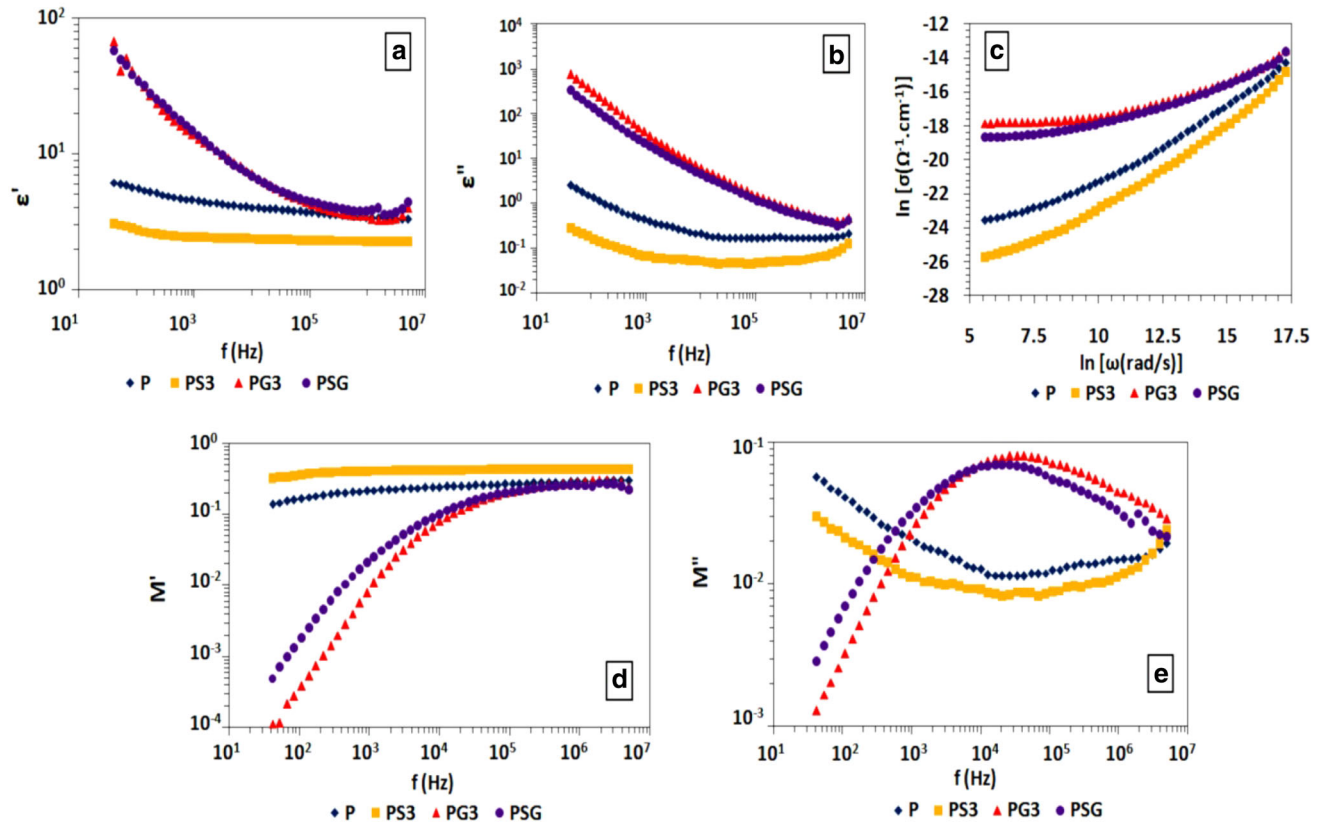
Fig. 5 Frequency dependence of **a** ε', **b** ε'', **c** σ_{AC}, **d** M', and **e** M'' for P, PS3, PG3, and PSG samples

**Table 3** Electrical parameters of P, PS3, PG3, and PSG samples

Sample	ε'(1 kHz)	ε''(1 kHz)	$\sigma_{DC}(\Omega^{-1}\,cm^{-1})$	M''_{max}	$f_{max}(10^4$ Hz)	$\tau(10^{-5}$ s)
P	4.56	0.45	6.8×10^{-11}	–	–	–
PS3	2.45	0.06	5.4×10^{-12}	–	–	–
PG3	13.94	39.54	1.8×10^{-8}	0.08	3.34	2.99
PSG	14.95	22.15	6.4×10^{-9}	0.07	1.63	6.12

3.4 Transmission and reflection spectra

Figure 6a and b represent the transmittance spectra of PVA/nSiO$_2$ and PVA/Gl composites, respectively. Concerning Fig. 6a, T% of sample P increases steeply in the UV range (200–380 nm) until it reaches a nearly constant value (89%) at 380 nm (i.e., in the visible range). Meanwhile, T% decreases as the SiO$_2$ content increases over the scanned wavelength range, according to the literature [11]. Such behavior will be discussed later along with reflectance data, to get a comprehensive understanding. On the other hand, T% data of PVA/Gl composites, illustrated in Fig. 6b, show that the glycerol content does not appreciably affect the transmittance of PVA.

To elucidate the effect of hard-soft hybrid filler mixing on the optical properties of PVA, a comparison of T% data of sample PSG to those of its relevant samples PS3, PG3, and P is presented in Fig. 7a. It is clear that PSG sample has much lower T% values in the UV range which reflects its higher UV resistance in comparison with P and PG3 samples. Moreover, T% of PSG increases dramatically as the wavelength increases till it reaches 63% at 600 nm, which is much higher than that of PS3 sample (14.5%) at the same wavelength. In other words, PSG sample has the advantage of being opaque to UV but transparent to visible light. For further illustration, Fig. 7b shows T% values of PSG, PS3, PG3, and P samples at 250 nm and 600 nm. Transmittance behavior of PSG sample
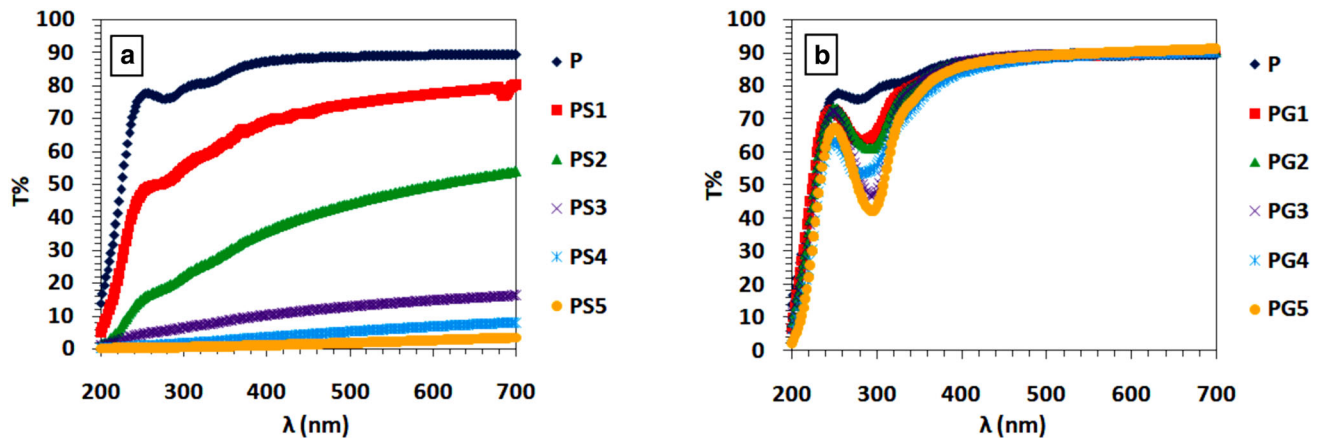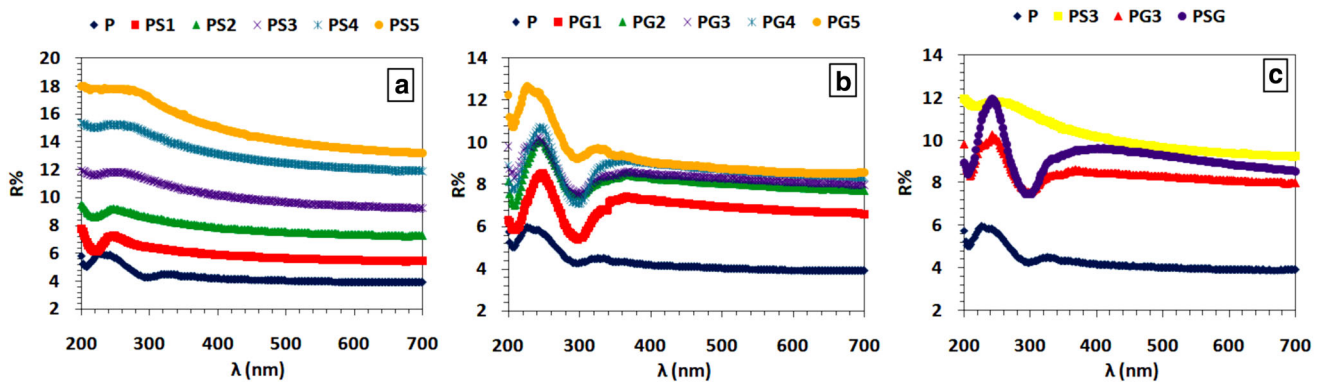
Fig. 6 Transmittance for **a** PVA/nSiO$_2$ composites and **b** PVA/Gl composites
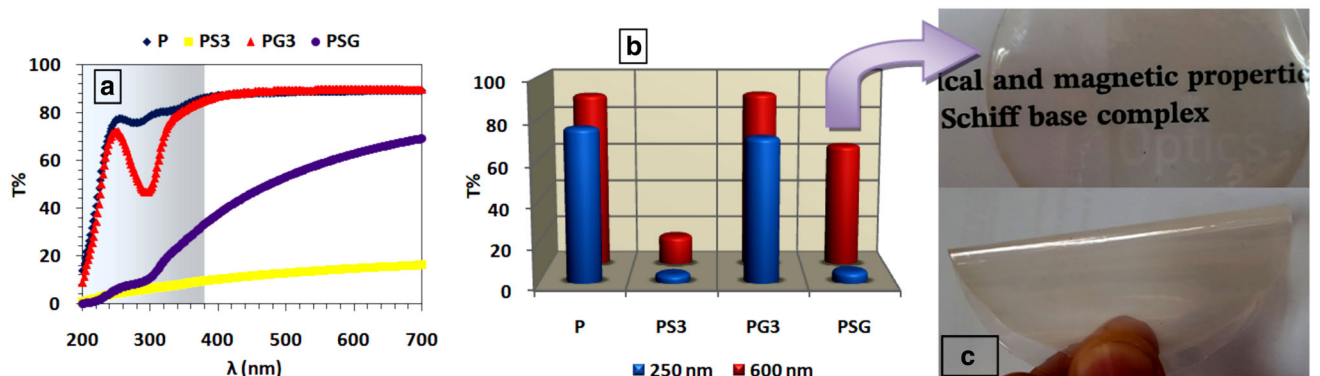
Fig. 7 **a** Transmittance for P, PS3, PG3, and PSG samples, **b** Transmittance for P, PS3, PG3, and PSG samples at 250 nm and 600 nm, and **c** Photograph of transparent PSG as a free-standing film

Fig. 8 Reflectance for **a** PVA/nSiO$_2$ composites, **b** PVA/Gl composites, and **c** P, PS3, PG3, and PSG samples

revealed its applicability as a transparent, biodegradable, and biocompatible UV-blocker.

Besides, Fig. 8a shows that sample (P) has low $R\%$ values over the whole spectrum with only small variations (6–4%). Meanwhile, $R\%$ increases as the nSiO$_2$ content increases over the scanned wavelength range (up to 14% at 600 nm for PS5). However, such

an increase in $R\%$ does not equate to the corresponding decrease in $T\%$ (from 89% for P sample to 2% for PS5 sample at 600 nm). Such decrease in $T\%$ for nSiO$_2$ loaded samples may thus be attributed to the increased light absorption caused by SiO$_2$ nanoparticles.

Similarly, glycerol addition slightly affects the reflectance of PVA (up to 9% at 600 nm for PG5), as shown in Fig. 8b. It is obvious that nSiO₂ showed a higher impact on the reflectance spectra of PVA than glycerol owing to the high reflectivity of SiO₂ nanoparticles. Consequently, R% spectra of PSG sample are close to that of PS3 sample, as presented in Fig. 8c.

3.5 Absorption studies

Optical absorption is investigated to obtain a deeper understanding of the prepared samples' electronic properties. The absorption coefficient (α) of a sample of thickness (t) at a certain wavelength (λ), neglecting multiple reflectances, is given by [45]:

$$\alpha = \frac{1}{t} \ln \left[\frac{(1-R)^2}{T} \right] \qquad (5)$$

The absorption coefficients (α) of PVA/nSiO₂ and PVA/Gl composites are presented as a function of light energy in Fig. 9a and b, respectively. An intense absorption is observed for all samples as the energy increases in the UV region, which is evidence of electronic transitions in this spectral region.

The spectrum of sample (P) reveals the existence of a π–π^* electronic transition that appears as an absorption band at 4.5 eV (276 nm). This transition owes to unhydrolyzed residues of carbonyl groups and ethylene groups present at the terminals of PVA polymeric chains [46]. Despite being damped upon nSiO₂ addition, these bands were, on contrary, enhanced by glycerol addition. The role of nSiO₂ and glycerol content in damping or enhancing the intensity of these bands will be discussed later using IR analysis.

However, sample (P) showed a sharp absorption edge (E_e) at 5.1 eV (240 nm), which shifted to lower energies with the increase in nSiO₂ content, as depicted in Fig. 9a. Consequently, a decrease in the calculated optical energy gap (E_g) of these samples is expected with the increase in nSiO₂ content [47]. On the other hand, such change was not observed in Fig. 9b for glycerol-loaded samples where the absorption edge showed undulated negligible changes. Instead, glycerol addition affected the absorption of pristine PVA in the UV region, which may be attributed to the increase in the charge carrier concentration by incorporating glycerol.

A deeper insight into the absorption spectra enables us to distinguish three regions; (i) a strong linear absorption region (Tauc's region), (ii) an exponential region (Urbach region), and (iii) a weak absorption tail.

The inspection of Tauc's region reveals the interband transitions between extended states of both valence and conduction bands. It thus provides an evaluation of the optical energy gap (E_g) according to the relation [48, 49]:

$$\alpha E_{ph} = B(E_{ph} - E_g)^m \qquad (6)$$

where (B) is a constant related to transition probability, (E_{ph}) is the energy of incident photons, and (m) is a power factor that refers to the mode of interband electronic transition. A direct allowed transition is distinguished by ($m = 0.5$), and indirect allowed one is denoted by ($m = 2$), whereas ($m = 1.5$) accounts for direct forbidden and ($m = 3$) accounts for indirect forbidden transitions.

On the other hand, additives and their induced defects inside a material cause a change in the band gap structure of the host material. New bands of
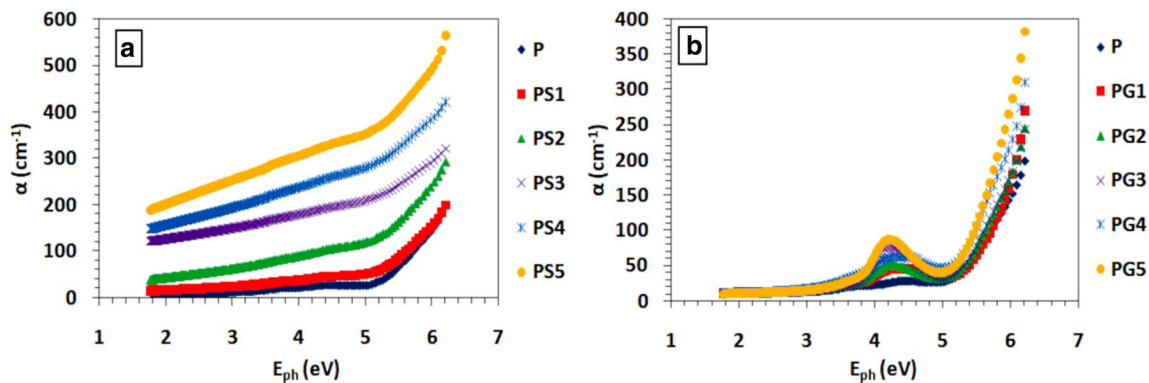

Fig. 9 Energy dependence of absorption coefficient for **a** PVA/nSiO₂ composites, and **b** PVA/Gl composites

localized states, caused by evoked disordering, will spread close to valence and conduction band edges and act as trapping and recombination centers. The width of these bands is known as Urbach energy (E_u) and can be estimated in the Urbach region by the relation:

$$\alpha = \alpha_o exp(\frac{E_{ph}}{E_u}) \tag{7}$$

In this context, evaluation of the band structure for samples P, PS3, PG3, and PSG can be derived by deducing their absorption edge (E_e), direct band gap (E_{gd}), indirect band gap (E_{gi}), and Urbach energy (E_u).

Plots of (α), (αE_{ph})$^{1/2}$, (αE_{ph})^2, and (ln α) against (E_{ph}) are shown in Fig. 10a–d. The values of E_e, E_{gd} and E_{gi} can be extracted from the intersection of the linear portion in the high absorption region with the x-axis in Fig. 10a–c, respectively. Meanwhile, E_u equals the reciprocal of the slope of the Urbach region in Fig. 10d.

It is obvious from summarized values in Table 4 that E_{gi} values are close to E_e and lower than E_{gd} for all samples. These results suggest that electronic

transitions, more probably, exhibit indirect rather than direct transitions for investigated samples.

Furthermore, sample P showed E_{gi} value of 5.1 eV and E_u value of 0.74 eV, which were altered by adding nSiO$_2$ as a result of induced defect levels within the band gap. The width of these levels had its highest value of 1.91 eV for PS3 sample with a resultant high reduction in E_{gi} to 3.2 eV. On the other hand, sample PG3 showed similar absorption behavior to that of sample P, except at the high energy region (UV), and also showed very close values of E_{gi} and E_u to those of sample P. These results confirm that glycerol barely affects the band structure of pure PVA but instead increases the charge carrier density. Accordingly, PSG sample

Table 4 Optical energy parameters of P, PS3, PG3, and PSG samples

Sample	E_e(eV)	E_{gi} (eV)	E_{gd} (eV)	E_u(eV)
P	5.1	5.1	5.8	0.74
PS3	3.2	3.2	5.2	1.91
PG3	5.1	5.2	5.7	0.75
PSG	4.2	4.6	5.4	1.41
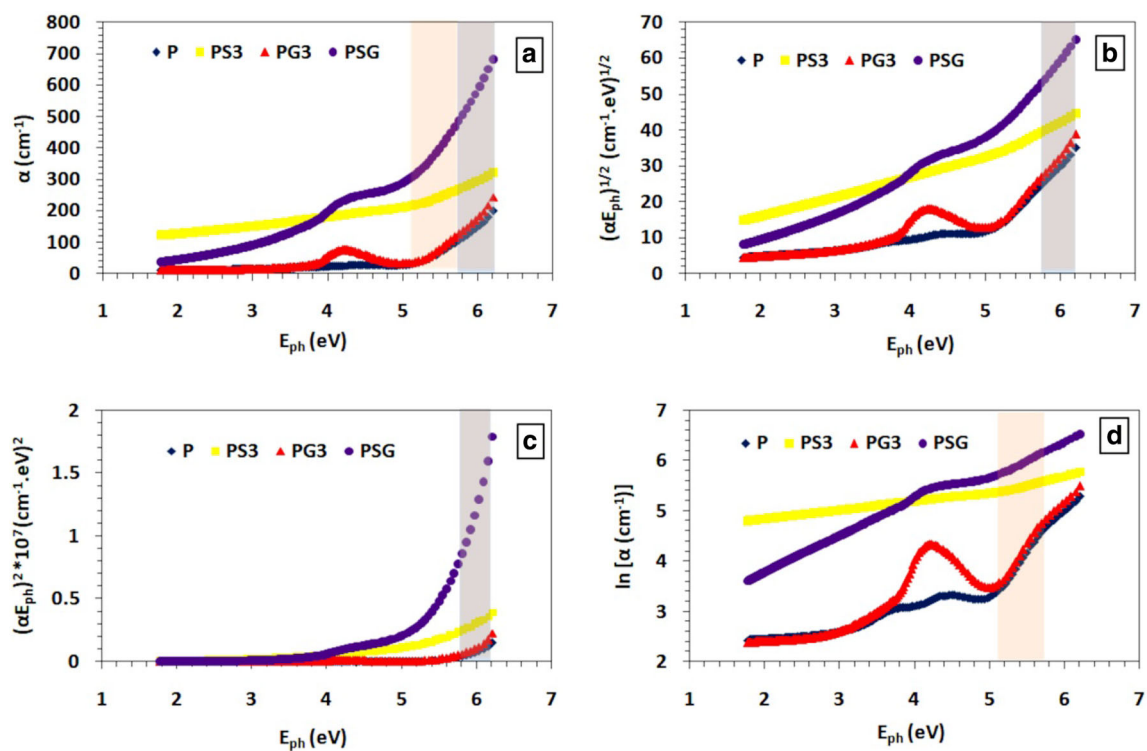
Fig. 10 Plots of **a** (α), **b** (αE_{ph})$^{1/2}$, **c** (αE_{ph})^2, and **d** (ln α) against (E_{ph}) for P, PS3, PG3, and PSG samples

showed the highest absorption behavior in the UV region (as seen in Fig. 10a), with increased band tail width (1.41 eV) and reduced band gap (4.6 eV).

3.6 Refractive index and dispersion

Regarding the fact that adhesives for optical components, optical waveguides, and anti-reflection coatings utilize materials of high refractive indices, the refractive index for our investigated samples is calculated as follows [45]:

$$n = \frac{1+R}{1-R} + \sqrt{\frac{4R}{(1-R)^2} - k^2} \qquad (8)$$

where $k = \frac{\alpha\lambda}{4\pi}$ is the extinction coefficient.

The effect of $nSiO_2$ and glycerol loadings on the refractive index of PVA at 600 nm (n_{600}) is depicted in Fig. 11a. It is clear that n_{600} values for both PVA/$nSiO_2$ and PVA/Gl composites are higher than that of neat PVA. Indeed, the refractive index increases upon increasing the packing density of a material. This fact interprets the increase in n upon incorporation of $nSiO_2$ in PVA because SiO_2 nanoparticles strongly interact with PVA leading to increased intermolecular packing, as confirmed by mechanical analysis. On contrary, mechanical analysis disproves this explanation in the case of PVA/Gl composites, as glycerol incorporation led to increased spacing between polymeric chains. In this case, it is more probable that the increased electronic polarizability within PVA/Gl composites led to a consequent increase in n [50].

Moreover, n_{600} was increased from 1.49 for PVA to 2.16 upon loading PVA with 15 wt% of $nSiO_2$, whereas it was raised up to 1.83 only for glycerol

loading of 30 wt%. As predicted by reflectance spectra, n for pure PVA was more sensitive to $nSiO_2$ addition than glycerol addition.

The wavelength (λ) dependence (400–600 nm) of refractive index (n) for samples P, PS3, PG3, and PSG is illustrated in Fig. 11b. It is obvious that sample PS3 has the highest n values. In contrast, samples PSG and PG3 showed higher values than neat PVA over the whole visible range.

Furthermore, Fig. 11b declares that n decreases with the increase in λ for all samples at different rates. The variation of n as a function of λ describes the optical dispersion of the material, which is an important parameter in the manufacturing of optical fibers. For the sake of simplicity, the dispersion of investigated samples will be evaluated qualitatively using a dimensionless factor known as "Abbe number" [50]:

$$V = \frac{(n_d - 1)}{(n_f - n_c)} \qquad (9)$$

where n_f, n_d, and n_c are the Fraunhofer spectral lines; (F = 486.1 nm), (D = 589.2 nm), and (C = 656.3 nm).

Surprisingly, V values are in the order PG3 > P > PS3 > PSG as tabulated in Table 5, with PSG sample having the highest dispersion (lowest V value).

3.7 Optoelectronic parameters

To evaluate the suitability of fabricated samples for different applications, estimation of optical dielectric constant, optical conductivity, and other optoelectronic parameters is crucial [50].
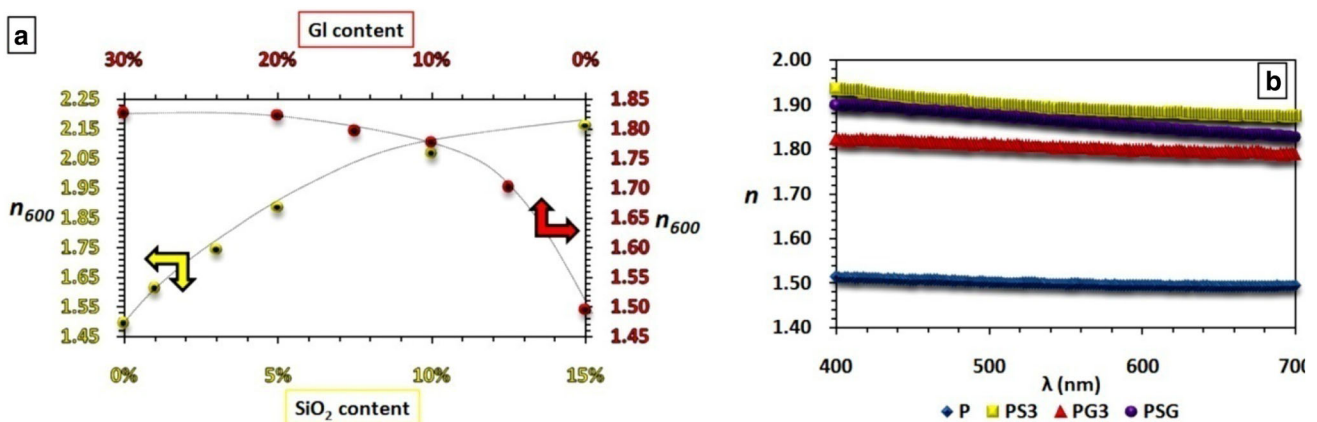

Fig. 11 a n_{600} as a function of $nSiO_2$ and Gl contents, and b wavelength dependence of n for P, PS3, PG3, and PSG samples

The optical conductivity of a material is described by the relation [51]:

$$\sigma_{(\lambda)} = \frac{\alpha n C}{4\pi} \qquad (10)$$

Figure 12a presents the effect of $nSiO_2$ and glycerol loadings on the optical conductivity of PVA at 600 nm (σ_{600}). Obviously, σ_{600} increases with the increase in the concentration of both additives but at a higher rate for $nSiO_2$ content than for glycerol content. The high sensitivity of σ_{600} to $nSiO_2$ addition owes to the high absorption of $nSiO_2$ particles.

Besides, Fig. 12b illustrates the wavelength dependence of optical conductivity for P, PS3, PG3, and PSG samples. The enhanced absorption of sample PSG in the UV range gives rise to enhanced optical conductivity in the same range, and thus sample PSG had the highest value of $\sigma_{(\lambda)}$. Afterward, the absorption of sample PSG decreases with the increase in wavelength till it intersects the PS3 sample's curve at 304 nm before decreasing again. However, the optical conductivity of PSG and PS3 samples are higher than those of samples P and PG3 over the whole range as the late mentioned samples have lower α and n values.

The real $\varepsilon'_{(\lambda)}$ and imaginary $\varepsilon''_{(\lambda)}$ parts of the optical dielectric constant are given by [51]:

$$\varepsilon'_{(\lambda)} = n^2 - k^2 \qquad (11)$$

$$\varepsilon''_{(\lambda)} = 2nk \qquad (12)$$

In fact, ε' and ε'' are related to the dispersion and rate of dissipation of electromagnetic waves, respectively. The two parameters can be utilized to calculate the energy losses at the surface and bulk of materials. The surface energy loss function (SELF) and volume energy loss function (VELF) are given by [52]:

$$\text{SELF} = \frac{\varepsilon''}{(\varepsilon' + 1)^2 + (\varepsilon'')^2} \qquad (13)$$

$$\text{VELF} = \frac{\varepsilon''}{(\varepsilon')^2 + (\varepsilon'')^2} \qquad (14)$$

However, SELF and VELF are calculated at 600 nm for P, PS3, PG3, and PSG samples and summarized in Table 5. Both types of losses were highest for PS3 sample, whereas samples P and PG3 attained the lowest values.

Furthermore, the dielectric constant at infinite frequency (ε_∞) can be estimated from the wavelength

Table 5 Dispersion and optoelectronic parameters of P, PS3, PG3, and PSG samples

Sample	V value	SELF	VELF	ε_∞	$N_c (10^{12}$ cm$^{-3})$
P	43.51	1.58×10^{-5}	3.31×10^{-5}	2.26	0.34
PS3	30.93	1.11×10^{-4}	1.82×10^{-4}	3.68	1.82
PG3	44.86	1.06×10^{-5}	1.82×10^{-5}	3.32	1.32
PSG	19.82	4.20×10^{-5}	7.02×10^{-5}	3.66	3.29
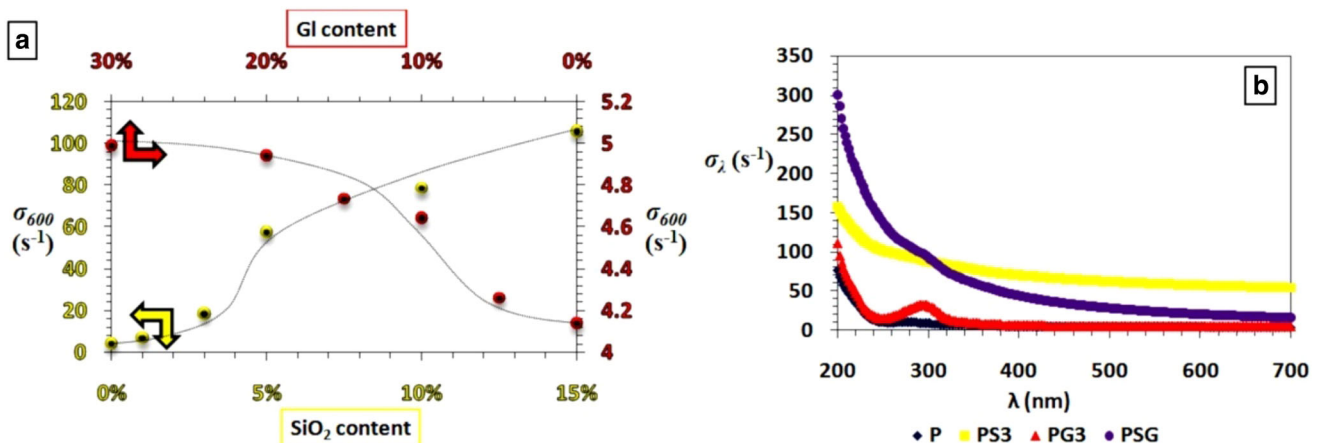
Fig. 12 **a** σ_{600} as a function of $nSiO_2$ and Gl contents, and **b** wavelength dependence of σ for P, PS3, PG3, and PSG samples

(λ) dependence of the real dielectric constant (ε') as follows [51]:

$$\varepsilon'_{(\lambda)} \approx \varepsilon_\infty - \frac{e^2 N_c}{\pi C^2 m^*} \lambda^2 \qquad (15)$$

Recalling that (C) is the speed of light, (e) is the electron charge, ($m^* = 0.44 m_e$) is the effective mass, and (m_e) is the electron mass; ε_∞ can be deduced as the intercept of ε' versus λ^2 plot and the charge carrier density (N_c) can be evaluated from the slope.

Figure 13 represents ε' versus λ^2 plots for P, PS3, PG3, and PSG samples, while the extracted ε_∞ and N_c values are gathered in Table 5. It is clear that all samples have higher ε_∞ and N_c values than neat PVA. Despite having close values of ε_∞, PSG has a higher N_c value than PS3 sample, as expected earlier by absorption studies.

3.8 IR analysis

FTIR spectra of PVA/nSiO$_2$ and PVA/Gl composites are collected in the spectral range (4000–600 cm^{-1}). To illustrate fine details of the spectra, it will be divided into three regions mainly; 3800–2600 cm^{-1}, 1800–1500 cm^{-1}, and 1500–600 cm^{-1}.

The pristine PVA exhibit three vibrational bands at 2851 cm^{-1}, 2910 cm^{-1}, and 3236 cm^{-1} which are assigned to C–H symmetric stretching, C–H asymmetric stretching, and O–H stretching vibrations, respectively, as shown in Fig. 14a–c [53]. The broadening of 3236 cm^{-1} band is attributed to the presence of multiple conformational positions of OH group

[54]. Thus the broadness alteration of 3236 cm^{-1} band by adding nSiO$_2$ and/or glycerol results from the modulation of hydrogen bonding structure (intramolecular to intermolecular).

Concerning the fact that polyvinyl alcohol results from hydrolysis of polyvinyl acetate, residues of unhydrolyzed acetate groups are responsible for three distinctive bands at 1592 cm^{-1}, 1656 cm^{-1}, and 1714 cm^{-1} even at low percent. These bands correspond to three resonating structures of the acetate group [50]. Besides, the 1592 cm^{-1} band may also be attributed to alkene C=C group residues [46].

It is evident from Fig. 15a that the 1592 cm^{-1} band disappeared upon increasing the nSiO$_2$ loading, whereas the 1656 cm^{-1} and 1714 cm^{-1} bands were slightly weakened and shifted to lower wave numbers 1646 cm^{-1} and 1705 cm^{-1}, respectively. The stabilization of the 1714 cm^{-1} band confirms the formation of intramolecular hydrogen bonds at C=O group [46]. On the other hand, Fig. 15b demonstrates the appearance of the three bands undiminished for all glycerol contents. The 1592 cm^{-1} band showed the largest redshift (1565–1574 cm^{-1}) with an increase in glycerol content. Recalling UV–Vis absorption studies; a π–π* electronic transition present at 276 nm in pure PVA was enhanced by glycerol addition. This behavior is consistent with the present findings of IR spectra. Proposed catalytic dehydration of glycerol into acrolein by the Brønsted acidic sites at 1592 cm^{-1} and 1646 cm^{-1} is responsible for the enhanced π–π* electronic transition of PVA/Gl composites [55]. For further illustration, the effect of nSiO$_2$ and/or

Fig. 13 ε' against λ^2 for P, PS3, PG3, and PSG samples
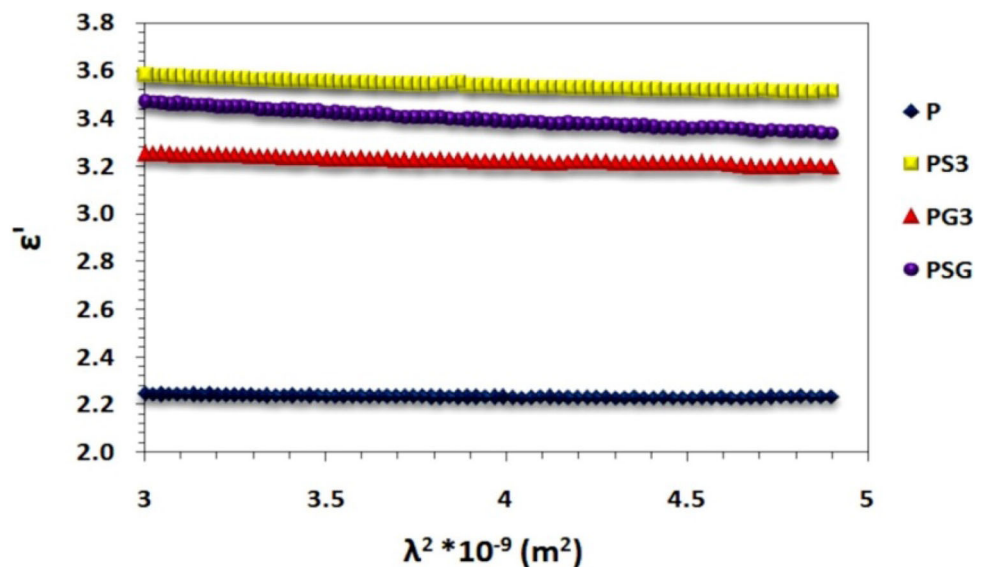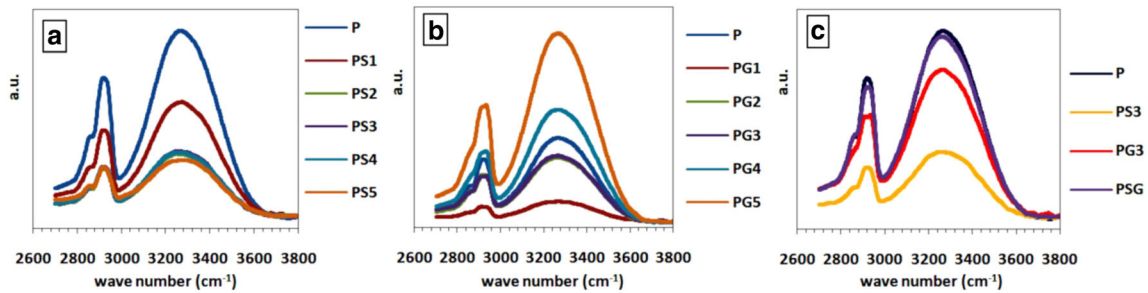
Fig. 14 IR spectra (3800–2600 cm^{-1}) for **a** PVA/nSiO$_2$ composites, **b** PVA/Gl composites, and **c** P, PS3, PG3, and PSG samples
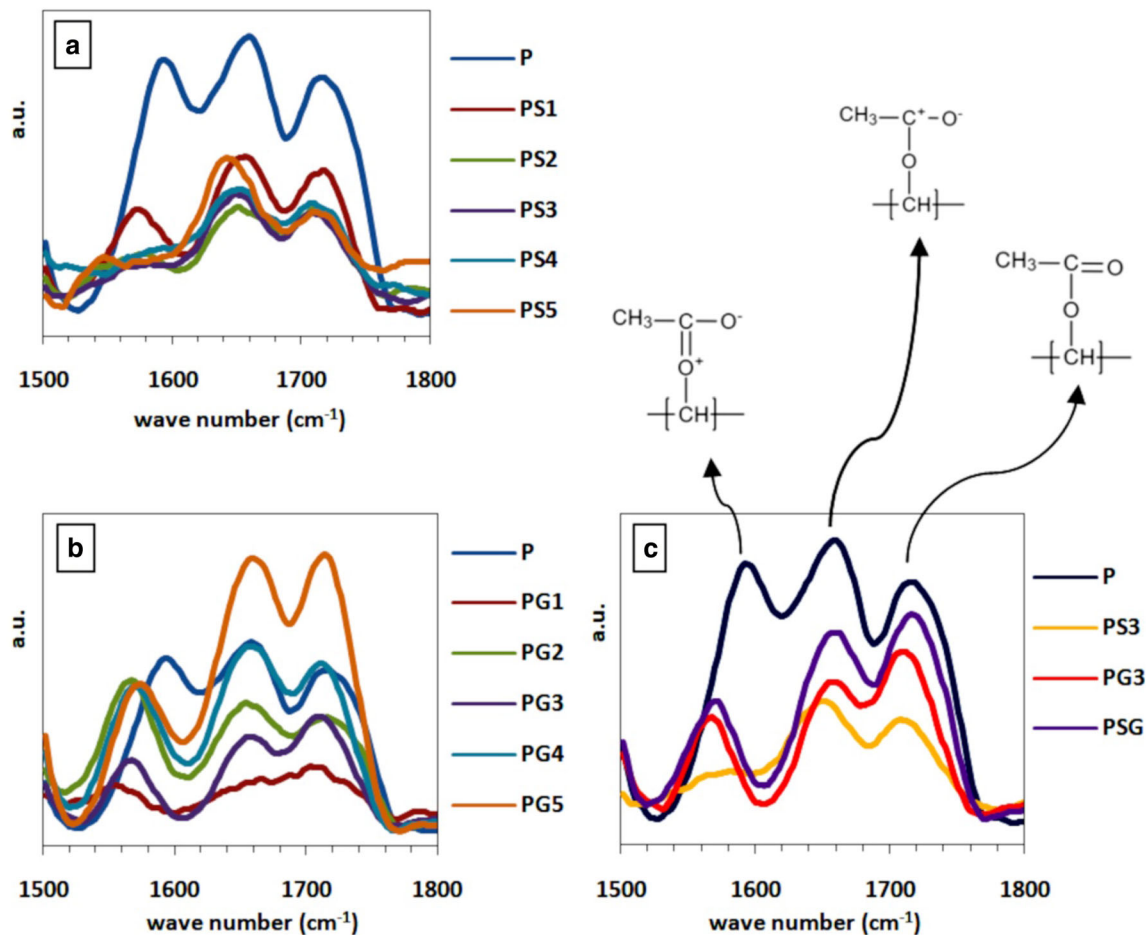
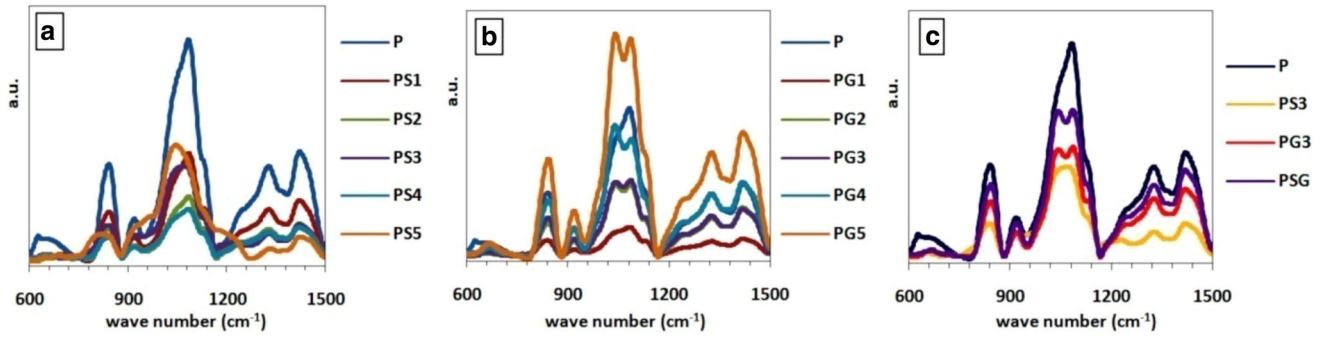

Fig. 15 IR spectra (1800–1500 cm^{-1}) for **a** PVA/nSiO$_2$ composites, **b** PVA/Gl composites, and **c** P, PS3, PG3, and PSG samples

glycerol addition to PVA on the IR spectra in this region along with resonating structures of the acetate group are depicted in Fig. 15c.

Additional vibrational bands of pure PVA present at 848 cm^{-1}, 920 cm^{-1}, 1089 cm^{-1}, 1269 cm^{-1}, 1339 cm^{-1}, and 1434 cm^{-1} belong, respectively, to C–H stretching, C–C stretching, C–O stretching, C–H wagging, C–H wagging and O–H bending, and C–H$_2$ stretching and O–H bending [56]. All glycerol-loaded samples showed observable splitting in the

Fig. 16 IR spectra (1500–600 cm^{-1}) for **a** PVA/nSiO$_2$ composites, **b** PVA/Gl composites, and **c** P, PS3, PG3, and PSG samples
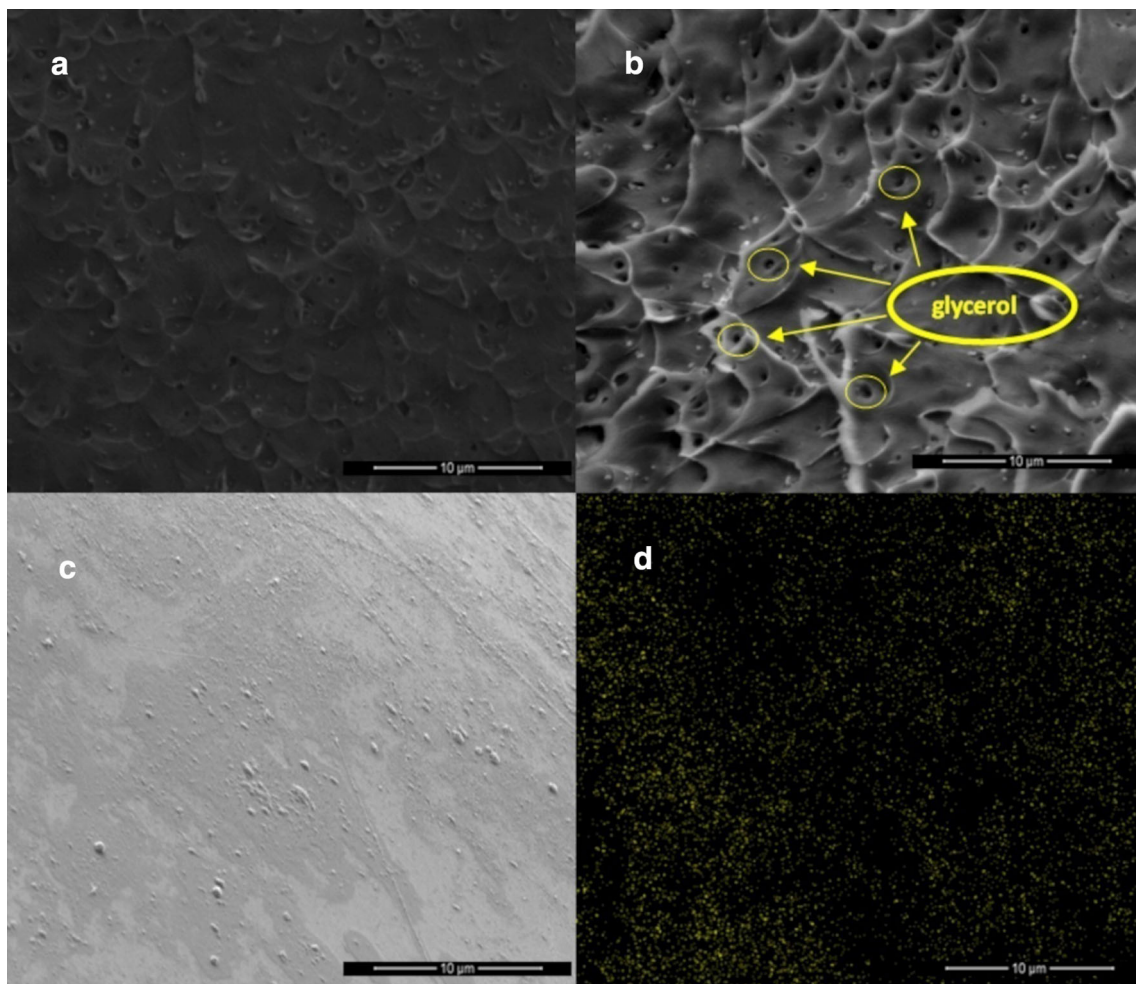
Fig. 17 SEM images of magnification × 10,000 for PSG sample **a** before treatment, **b** after treatment with ethanol, **c** surface, and **d** EDX mapping of Si element

1089 cm^{-1} band with an additional band at 1036 cm^{-1}, as illustrated in Fig. 16a–c, which owes to the C–O stretching of glycerol.

3.9 SEM characterization

Cross-sectional SEM analysis of polymeric films has the privilege of exploring layer formation, pore formation,

air voids, and filler distribution in the bulk of the film. Figure 17a illustrates a cross-sectional SEM micrograph of the PSG sample. Firstly, there is no evident particle agglomeration or layer separation in the micrograph. Afterward, a fractured part of the sample was lightly immersed in ethanol before being dried under vacuum for 15 min. A cross-sectional SEM micrograph, presented in Fig. 17b, was explored after ethanol treatment. The micrograph depicts the formation of micropores of homogeneous diameters, which is attributed to glycerol content extracted by ethanol. This finding reveals that the glycerol content in PSG sample was not totally interacted with PVA and confirms the plasticizing effect of glycerol as investigated by mechanical analysis. A surface SEM image of PSG and its relevant EDX mapping of Si element are explored in Fig. 17c and d, respectively, to represent the homogeneous distribution of $nSiO_2$ particles in the PVA matrix.

4 Conclusion

A PVA composite of hard-soft hybrid filler ratio 1:3 ($nSiO_2$:Gl) was prepared by casting, in addition to two separate series of PVA/$nSiO_2$ and PVA/glycerol composites. The effect of hybrid filler as well as individual fillers on the mechanical, electrical, and optical properties of PVA is investigated.

The glycerol content in the hybrid sample showed higher impact on the storage modulus than $nSiO_2$ content does and the sample is eventually flexible.

Dielectric properties of PVA/$nSiO_2$ composites showed anomalous behavior. Meanwhile, glycerol addition manifests a percolative behavior of conductivity. The glycerol effect on the electrical properties in the hybrid sample is dominant. The modified Jonscher equation is fitted to measured AC conductivity of glycerol-loaded samples whereas electric modulus formalism is utilized to explain existed relaxations. Calculated relaxation times infer that glycerol molecules were highly free and facilitate the segmental motion of polymeric chains.

Transmittance studies in the UV–Vis range revealed that hybrid sample has the advantage of being opaque to UV light but transparent to visible light. This finding represents the applicability of the film as a transparent, biodegradable, and biocompatible UV resistant material. The hybrid sample is characterized also by lower energy gap than pure PVA while exhibits higher Urbach tail, refractive index, optical conductivity, optical dielectric constant, and charge carrier density.

Remarkably, glycerol addition enhances the flexibility and electric conductivity of PVA/$nSiO_2$ composites without distorting their optical properties, as the optical properties are more sensitive to the $nSiO_2$ content.

Author contributions

Conceptualization, methodology, writing, review, and editing were performed by EM. Measurements and material preparation were done by EOT.

Data availability

All data generated or analyzed during this study are included in this published article.

Declarations

Conflict of interest The authors have no relevant financial or non-financial interests to disclose.

References

1. D.W. Lee, B.R. Yoo, J. Ind. Eng. Chem. **38**, 1 (2016)
2. H. Zou, S. Wu, J. Shen, Chem. Rev. **108**, 3893 (2008)
3. T.S. Soliman, S.A. Vshivkov, S.I. Elkalashy, Polym. Compos. **107**, 110037 (2020)
4. S. Choudhary, J. Mater. Sci. Mater. Electron. **29**, 10517 (2018)
5. A.M. Alsaad, A.A. Ahmad, A.R. Al-Dairy, A.S. Al-anbar, Q.M. Al-Bataineh, Results Phys. **19**, 103463 (2020)
6. S. El-Sayed, T. Abel-Baset, A.A. Elfadl, A. Hassen, Phys. B Condens. Matter **464**, 17 (2015)
7. R.-J. Zhou, T. Burkhart, J. Thermoplast. Compos. Mater. **23**, 487 (2010)
8. H. Althues, J. Henle, S. Kaskel, Chem. Soc. Rev. **36**, 1454 (2007)
9. M.C. Popescu, Int. J. Biol. Macromol. **101**, 783 (2017)
10. J. Tian, R. Fan, Z. Zhang, Y. Li, H. Wu, P. Yang, P. Xie, W. Duan, C.-S. Lee, J. Mater. Sci. Technol. **131**, 91 (2022)
11. B. Karthikeyan, S. Hariharan, A. Sasidharan, V. Gayathri, T. Arun, A. Akbari-Fakhrabadi, C. Madhumitha, Opt. Mater. (Amst). **90**, 139 (2019)
12. K. Deshmukh, M.B. Ahamed, K.K. Sadasivuni, D. Ponnamma, M.A.A. Al-Maadeed, R.R. Deshmukh, S.K.K. Pasha, A.R. Polu, K. Chidambaram, J. Appl. Polym. Sci. (2017). https://doi.org/10.1002/app.44427
13. O. Esim, S. Kurbanoglu, A. Savaser, S.A. Ozkan, Y. Ozkan, *New Developments in Nanosensors for Pharmaceutical Analysis* (Academic Press, Cambridge, 2019), pp.273–301
14. S. Choudhary, R.J. Sengwa, AIP Conf. Proc. **1728**, 020425 (2016)
15. Z.M. Dang, J.K. Yuan, J.W. Zha, T. Zhou, S.T. Li, G.H. Hu, Prog. Mater. Sci. **57**, 660 (2012)
16. Y. Shen, Z. Yue, M. Li, C.W. Nan, Adv. Funct. Mater. **15**, 1100 (2005)
17. L. Qi, B.I. Lee, W.D. Samuels, G.J. Exarhos, S.G. Parler, J. Appl. Polym. Sci. **102**, 967 (2006)
18. A. Pal, A. Sasmal, B. Manoj, D.P. Rao, A.K. Haldar, S. Sen, Mater. Chem. Phys. **244**, 122639 (2020)
19. Z.M. Dang, L.Z. Fan, Y. Shen, C.W. Nan, Chem. Phys. Lett. **369**, 95 (2003)
20. J. Liu, G. Tian, S. Qi, Z. Wu, D. Wu, Mater. Lett. **124**, 117 (2014)
21. C. Huang, Q.M. Zhang, G. DeBotton, K. Bhattacharya, Appl. Phys. Lett. **84**, 4391 (2004)
22. G. Wang, ACS Appl. Mater. Interfaces **2**, 1290 (2010)
23. Y. Li, X. Huang, Z. Hu, P. Jiang, S. Li, T. Tanaka, ACS Appl. Mater. Interfaces **3**, 4396 (2011)
24. J. Pu-you, B. Cai-ying, H. Li-hong, Z. Yong-hong, J. For. Prod. Ind. **3**, 151 (2014)
25. M. Mohsin, A. Hossin, Y. Haik, J. Appl. Polym. Sci. **122**, 3102 (2011)
26. L.T. Sin, W.A. Rahman, A.R. Rahmat, N.A. Morad, M.S.N. Salleh, Pertanika. J. Sci. Technol. **18**, 387 (2010)
27. G. Ayala, A. Agudelo, R. Vargas, Dyna **171**, 138 (2012)
28. P. Mazurek, S. Hvilsted, A.L. Skov, Polymer (Guildf). **87**, 1 (2016)
29. P. Mazurek, L. Yu, R. Gerhard, W. Wirges, A.L. Skov, J. Appl. Polym. Sci. **133**, 88 (2016). https://doi.org/10.1002/app.44153
30. S. Zakaria, A.F.A. Osman, S.N.H. Mustapha, L.K. Yiew, AIP Conf. **2030**, 020183 (2018)
31. M. Abu-Abdeen, J. Appl. Polym. Sci. **124**, 3192 (2012)
32. K. Chrissafis, K.M. Paraskevopoulos, G.Z. Papageorgiou, D.N. Bikiaris, J. Appl. Polym. Sci. **110**, 1739 (2008)
33. L.A. Pothan, S. Thomas, G. Groeninckx, Compos. Part A Appl. Sci. Manuf. **37**, 1260 (2006)
34. D.I. Bower, *An Introduction to Polymer Physics* (Cambridge University Press, Cambridge, 2003)
35. J. Segur, J. Agric. Food Chem. **1**, 567 (1953)
36. J.P. Tiwari, K. Shahi, Philos. Mag. **87**, 4475 (2007)
37. K. Sun, W. Duan, Y. Lei, Z. Wang, J. Tian, P. Yang, Q. He, M. Chen, H. Wu, Z. Zhang, R. Fan, Compos. Part A Appl. Sci. Manuf. **156**, 106854 (2022)
38. Z. Wang, K. Sun, H. Wu, Y. Qu, J. Tian, L. Ju, R. Fan, Compos. Sci. Technol. **227**, 109600 (2022)
39. Y. Pu, Z. Dong, P. Zhang, Y. Wu, J. Zhao, Y. Luo, J. Alloys Compd. **672**, 64 (2016)
40. Z. Wang, K. Sun, Y. Qu, Z. Wang, J. Tian, X. Li, R. Fan, Mater. Des. **209**, 110009 (2021)
41. B. Hilker, K.B. Fields, A. Stern, B. Space, X.P. Zhang, J.P. Harmon, Polymer (Guildf). **51**, 4790 (2010)
42. P. Dhatarwal, R.J. Sengwa, Mater. Res. Bull. **129**, 110901 (2020)
43. C. Rayssi, S. El Kossi, J. Dhahri, K. Khirouni, RSC Adv. **8**, 17139 (2018)
44. T.A. Hanafy, J. Appl. Phys. **112**, 34102 (2012)
45. J.S. Jan-Mistrik, S. Kasap, H.E. Ruda, C. Koughia, *Springer Handbook of Electronic and Photonic Materials*, 2nd edn. (Springer, Cham, 2017)
46. K.M. Abd-El-Kader, J. Appl. Polym. Sci. **88**, 589 (2003)
47. D.L. Wood, J.S. Tauc, Phys. Rev. B **5**, 3144 (1972)
48. J. Tauc, in *Amorphous and liquid semiconductors*. ed. by J. Tauc (Springer US, Boston, 1974), pp.159–220
49. N.F. Mott, E.A. Davis, *Electronic Processes in Non-Crystalline Materials* (Oxford University Press, Oxford, 2012)
50. M. Banerjee, A. Jain, G.S. Mukherjee, Polym. Compos. **40**, E765 (2019)
51. M. Kahouli, A. Barhoumi, A. Bouzid, A. Al-Hajry, S. Guermazi, Superlattices Microstruct. **85**, 7 (2015)

52. R.M. Ahmed, M.M. Atta, E.O. Taha, J. Mater. Sci. Mater. Electron. **32**, 22699 (2021)

53. N. Peppas, Die Makromol. Chem. **178**, 595 (1977)

54. M.L. Hallensleben, R. Fuss, F. Mummy, Ullmann's Encycl. Ind. Chem. **1**, 1–23 (2015)

55. I.P. Rosas, J.L. Contreras, J. Salmones, C. Tapia, B. Zeifert, J. Navarrete, T. Vázquez, D.C. García, Catalysts **7**, 73 (2017)

56. L. Dai, J. Li, E. Yamada, J. Appl. Polym. Sci. **86**, 2342 (2002)